# On the role of coupled-clusters' full triple and perturbative quadruple excitations on rovibrational spectra of van der Waals complexes

Piotr Jankowski<sup>a</sup>, Ewelina Grabowska<sup>a</sup>, and Krzysztof Szalewicz<sup>b</sup>

- <sup>a</sup> Faculty of Chemistry, Nicolaus Copernicus University in Toruń, Gagarina 7, 87-100 Toruń, Poland
- <sup>b</sup> Department of Physics and Astronomy, University of Delaware, Newark, DE 19716

### ARTICLE HISTORY

Compiled June 22, 2021

#### ABSTRACT

The importance of coupled clusters iterative triple and noniterative quadruple, T(Q), electron excitations on the potential energy surfaces (PESs) of van der Waals molecules is examined for  $H_2$ –CO. Evaluation of this importance is performed by comparing theoretical spectra with experiment. Somewhat surprisingly, although the T(Q) contributions to interaction energies are below 3%, the inclusion of them reduces the error of theory with respect to experiment by an order of magnitude and qualitative agreement of the spectra in some regions is achieved only when they are included. The main reason for these observations is that the T(Q) effects significantly change the anisotropy of the PES.

## 1. Introduction

Small van der Waals clusters are important systems for improving the understanding of intermolecular interactions by interplay of theory and experiment. On one hand, very accurate spectra of such systems are often available. On the other hand, *ab initio* electronic structure calculations of potential energy surfaces (PESs) can be performed at high levels of theory with extrapolations to complete basis set (CBS) limits and quantum nuclear dynamics calculations can be performed essentially exactly and including all degrees of freedom. Therefore, comparisons of theoretical spectra with experiment provide a stringent evaluation of the importance of various physical components of intermolecular interactions and of methods used to compute these components. This information is important for theoretical predictions for larger systems where accuracy of theory has to be reduced and it is important to select optimal theory levels and to be able to estimate its uncertainties. Conversely, high-accuracy calculations can be used to interpret experimental spectra. Examples of interplay between *ab initio* theory and experiment for van der Waals clusters can be found in Refs. [1–22].

The class of small van der Waals clusters can be defined as clusters containing up to 6 atoms. The full-dimensional PESs for such clusters include up to 12 degrees of freedom, which is the current limit for performing quantum nuclear dynamics calculations [23, 24. The electronic structure approach most often used in developments of PESs for such clusters is the coupled clusters method with single, double, and noniterative triple excitations, CCSD(T), Refs. [25–29]. This method is computationally fairly efficient as it scales as  $\mathcal{O}(N^7)$  with system size and at the same time predicts interaction energies with uncertainties of a couple percent at the CBS limit [15, 30–32]. In fact, CCSD(T) has been shown in numerous applications to be a very reliable method to predict properties (even for excited states [33]) for all types of molecular systems that can be well approximated by a single Hartree-Fock (HF) determinant and therefore it is often called the "gold standard" of electronic structure calculations. Obviously, there are also properties that require going beyond CCSD(T) in terms of electron excitations. The consecutive steps in the inclusion of such excitations are the iterated triple excitations in CCSDT [34, 35] and the noniterated quadruple excitations in CCSDT(Q) [36]. These methods are, however, much more expensive than CCSD(T) since they scale as  $\mathcal{O}(N^8)$  and  $\mathcal{O}(N^9)$ , respectively. Despite such steep scaling, both methods found extensive applications in theoretical calculations of isolated-molecule spectra [37–42] and in thermochemistry [43, 44].

The effects of T(Q) excitations have also been investigated in theory of intermolecular interactions and the inclusion of such excitations is sometimes considered to be a part of the "platinum standard" [45] (which also adds the Born-Oppenheimer diagonal correction and relativistic effects). The T(Q) terms have been included in calculations for a number of dimers, but in most cases only at a few selected points on a PES [31, 32, 46–50]. To our knowledge, for clusters containing more than two atoms the only PES including the T(Q) excitations was developed for  $H_2$ —CO in Refs. [15, 30]. One should mention here that for up to four-electron systems consisting of three or four lightest atoms, full configuration interaction (FCI) calculations are possible. PESs including FCI contributions have been developed for  $H_2$ — $H_2$  in Refs. [51, 52] and for  $H_2$ — $H_2$  in Refs. [53, 54]. The T(Q) contributions not only scale as  $\mathcal{O}(N^9)$ , but also converge slowly with basis set and the use of augmented double-zeta basis sets results in 35% average error for a set of 21 small dimers relative to CBS limits computed in larger basis sets [55]. This error is actually not much larger than the relative errors of the CCSD(T) level in the same basis set. However, CCSD(T) calculations can be

performed in basis sets up to quintuple-zeta quality, which reduces the errors to below 1%, while the T(Q) effects cannot currently be computed in increased-size basis sets for all grid points required to fit the complete PES. Nevertheless, due to the smallness of the T(Q) contribution to the interaction energy compared to the CCSD(T) contribution, the absolute uncertainties in both quantities are close to each other.

As stated above, the T(Q) contributions have been used in the development of the  $H_2$ –CO PES in Refs. [15, 30], and the effects of these corrections on the interaction energies, in particular in the regions of the global and local minima, have been discussed in these references (and also in Ref. [56]). However, the effects on spectra could not be determined since several other aspects of the PES have been improved at the same time. The overall effect of all these improvements was that the theoretical spectrum of  $H_2$ –CO agreed very well with experiment and allowed for the first time to interpret the spectrum of  $orthoH_2$ –CO, that had been measured a decade earlier. In the present paper, we have developed a new PES at the CCSD(T) level of theory. In all other respects this PES is identical to that of Refs. [15, 30], so one may also view it as the latter PES with the T(Q) effects subtracted. Comparisons of the spectra computed from both surfaces with the experimental spectrum allows one to evaluate the role of these effects on the final outcome of theory: observable quantities.

# 2. Potential energy surface

To describe the geometry the H<sub>2</sub>–CO complex, one can use the coordinate system with the intermolecular coordinates  $\mathbf{X} = (R, \theta_1, \theta_2, \phi)$  and the intramolecular ones  $(r_1, r_2)$ , where R denotes the distance between the centers of mass (COM) of monomers. The COM of H<sub>2</sub> is placed at the origin of the coordinate system and the COM of CO at z = R. Then  $\theta_1$  ( $\theta_2$ ) denotes the angle between the vector starting at the appropriate COM and ending up in H (C) and the  $\hat{z}$  axis,  $\phi$  is the dihedral angle between these vectors, whereas  $r_1$  and  $r_2$  are the interatomic separations in H<sub>2</sub> and CO, respectively.

To reach our goal, i.e., to find the effect of the T(Q) contributions on the quality of the rovibrational spectra of  $H_2$ –CO, we need two surfaces: the one with the highest possible excitation level included and the other one which differs only by the lower level of excitations, namely the CCSD(T) level. As the former surface, we will use the  $V_{12}$  surface developed in Ref. [15], the latter surface was obtained in the present paper. The  $V_{12}$  surface was fitted to the *ab initio* interaction energies calculated on the full, six-dimensional (6D) grid. At each grid-point in intermolecular coordinates X, the PES was expressed as Taylor's expansion in powers of  $r_1$  and  $r_2$ . These interaction energies were averaged over the monomers' vibrations at each X

$$\langle V \rangle_{v_1 v_2}(\boldsymbol{X}) = f_{00}^c(\boldsymbol{X}) + f_{10}^c(\boldsymbol{X})(\langle r_1 \rangle_{v_1} - r_{1c}) + f_{01}^c(\boldsymbol{X})(\langle r_2 \rangle_{v_2} - r_{2c}) + f_{11}^c(\boldsymbol{X})(\langle r_1 \rangle_{v_1} - r_{1c})(\langle r_2 \rangle_{v_2} - r_{2c}) + \frac{1}{2} f_{20}^c(\boldsymbol{X})(\langle r_1^2 \rangle_{v_1} - 2r_{1c}\langle r_1 \rangle_{v_1} + r_{1c}^2) + \frac{1}{2} f_{02}^c(\boldsymbol{X})(\langle r_2^2 \rangle_{v_2} - 2r_{2c}\langle r_2 \rangle_{v_2} + r_{2c}^2),$$

$$(1)$$

where  $f_{ij}^c$  are the *i*-th and *j*-th numerical derivatives with respect to the  $r_1$  and  $r_2$  coordinates, calculated at the reference intramolecular separations  $r_{1c}$  and  $r_{2c}$ , respectively. The averaging is done over the wave functions of the  $v_1$ -th vibrational state of  $H_2$  and the  $v_2$ -th vibrational state of  $H_2$  or  $H_2$  are the interval of  $H_2$  and the  $H_3$  are the interval of  $H_3$  are the interval of  $H_3$  and the interval of  $H_3$  are the interval of  $H_3$  and the interval of  $H_3$  are the interval of  $H_3$  and  $H_4$  are the interval of  $H_3$  and  $H_4$  are the interval of  $H_4$  and  $H_4$  are the interva

values of powers of intramonomer distances  $\langle r_1^n \rangle_{v_1}$  and  $\langle r_2^n \rangle_{v_2}$  in Eq. 1. To calculate the infrared spectra, we actually need two vibrationally averaged surfaces  $\langle V \rangle_{00}$  and  $\langle V \rangle_{01}$ . The leading term in the expansion (1),  $f_{00}^c(\boldsymbol{X})$ , is the interaction energy calculated for the reference intramonomer separations  $r_{1c}$  and  $r_{2c}$ . This quantity was obtained at a high level of theory (indicated by the subscript H below)

$$E_{\text{int,H}} = E_{\text{int}}^{\text{HF}}[5] + \delta E_{\text{int}}^{\text{CCSD(T)}}[\text{Q5}] + \delta E_{\text{int}}^{\text{T(Q)}}[\text{D}], \tag{2}$$

where  $E_{\rm int}^{\rm HF}[5]$  is the interaction energy calculated at the HF level using the aug-cc-pVXZ basis set [57] with X=5.  $\delta E_{\rm int}^{\rm CCSD(T)}[{\rm Q5}]$  denotes the correlation contribution to the all-electron CCSD(T) interaction energy with the complete basis set (CBS)  $1/X^3$  extrapolations [58] from the aug-cc-pVQZ and aug-cc-pV5Z basis sets, and

$$\delta E_{\rm int}^{\rm T(Q)}[{\rm D}] = E_{\rm int}^{\rm CCSDT(Q)}[{\rm D}] - E_{\rm int}^{\rm CCSD(T)}[{\rm D}]$$
 (3)

accounts for the electron correlation effects at the level of CCSDT(Q), computed in the aug-cc-pVDZ basis set using the frozen-core approximation (in this case, the CCSD(T) contribution in Eq. (3) also utilized this approximation). The derivatives  $f_{ij}^c(\mathbf{X})$  with i+j>0 were calculated at a lower, 'base' level of theory, denoted by the subscript B:

$$E_{\text{int,B}} = E_{\text{int}}^{\text{HF}}[Q] + \delta E_{\text{int}}^{\text{CCSD(T)}}[TQ],$$

using notation analogous to that in Eq. (2). It has been shown in Ref. [30] that the lower level of theory used to calculate  $f_{ij}^c(\mathbf{X})$ , i+j>0, introduces negligible errors in these derivatives.

In order to evaluate the importance of the  $\delta E_{\rm int}^{\rm T(Q)}$  effect, we developed in the present work a surface fitted to the CCSD(T)-theory level.

$$E'_{\text{int,H}} = E_{\text{int}}^{\text{HF}}[5] + \delta E_{\text{int}}^{\text{CCSD(T)}}[Q5]. \tag{4}$$

The leading term in formula (1),  $f_{00}^c$ , is represented by  $E'_{\rm int,H}$ , while the other terms are the same as those used for  $V_{12}$ . Such training data were fitted by exactly the same analytic form of the potential energy surface as that used to fit  $V_{12}$ . The resulting surface will be further denoted as  $V_{\rm nT(Q)}$ , where  $\rm nT(Q)$  indicates that "no  $\rm T(Q)$ " contribution is included. We use this notation to emphasize that the only purpose of this PES is the investigation of the role of the  $\rm T(Q)$  effects. We can expect that the quality of the  $V_{\rm nT(Q)}$  fit is very similar to that of  $V_{12}$  since we have used the same grid points, the same functional form, the same weighting functions, and the same optimization procedure. Thus, the only reason for the differences between  $V_{\rm nT(Q)}$  and  $V_{12}$  comes from the absence of the  $\delta E_{\rm int}^{\rm T(Q)}$  correction in the former case. Similarly to the  $V_{12}$  surface, we have obtained two versions of  $V_{\rm nT(Q)}$ , for the  $v_2 = 0$  and  $v_2 = 1$  vibrational states of CO.

The magnitude of the  $\delta E_{\rm int}^{\rm T(Q)}$  contribution, along with the individual  $\delta E_{\rm int}^{\rm T}$  and  $\delta E_{\rm int}^{\rm (Q)}$  components, was studied in Ref. [30] for a few geometries. Now we can compare  $V_{\rm nT(Q)}$  and  $V_{12}$  for any intermolecular geometry. First, we can check the positions and the energies of the global and local minima, see Table 1. For  $V_{\rm nT(Q)}$ ,  $v_2 = 0$ , the global minimum is shallower by 2.83 cm<sup>-1</sup> and the position of the minimum is shifted by 0.02 bohr relative to the  $V_{12}$  value. For the local minimum, the corresponding values are 0.76

cm<sup>-1</sup> and 0.01 bohr. The differences are similar for  $v_2 = 1$ . The comparison of these two minima shows that the addition of  $\delta E_{\rm int}^{\rm T(Q)}$  changes the anisotropy of the surface. To see this effect on anisotropy for a broader range of intermolecular geometries, we plotted in Fig. 1 the angular dependence of  $V_{\rm nT(Q)} - V_{12}$  for two intermolecular separations R and a few values of  $(\theta_2, \phi)$ , panels A and C, and  $(\theta_1, \phi)$ , panels B and D. To demonstrate how large are these differences relative to the total interaction energy, the values of  $V_{\rm nT(Q)}$  are also plotted. Since differences are small in comparison with the absolute values of the energies, we use different scales of energies for each of these quantities. In panel D, one can see how  $V_{\rm nT(O)} - V_{12}$  changes when moving away from the vicinity of the global minimum,  $(R, \theta_1, \theta_2, \phi) = (8.0, 0^{\circ}, 180^{\circ}, 0^{\circ})$ , by decreasing the angle  $\theta_2$ . Upon such changes of  $\theta_2$ , the value of  $V_{\rm nT(Q)} - V_{12}$  gradually decreases from 2.65 cm<sup>-1</sup>, for  $\theta_2 = 180^{\circ}$ , to 0.26 cm<sup>-1</sup> for  $\theta_2 = 0^{\circ}$ , whereas the value of  $V_{\rm nT(Q)}$  decreases from -91.0 cm<sup>-1</sup> to -55.5 cm<sup>-1</sup>, respectively. Thus, the inclusion of  $\delta E_{\rm int}^{\hat{T(Q)}}$  enhances the anisotropy of the potential by about 2.4 cm<sup>-1</sup>, which amounts to 2.6% of the interaction energy in the vicinity of the global minimum. The ratios  $E_{\rm int}(180^{\circ})/E_{\rm int}(0^{\circ})$  are 1.64 and 1.68 for  $V_{\rm nT(Q)}$  and  $V_{12}$ , respectively. Also the other panels of Fig. 1 show a strong dependence of  $\delta E_{\rm int}^{\rm T(Q)}$  on the angular orientation of the interacting molecules. Although the effects of  $\delta E_{\rm int}^{\rm T(Q)}$  may not appear to be large in terms of anisotropy ratios, they do introduce quite substantial changes in the spectra, see Section 3.

## 3. Calculation of the spectra

The  $V_{12}$  interaction energy surface was very successful in predicting the infrared [15, 30] and millimeter-wave [30] spectra for both the para and  $orthoH_2$ —CO dimers. Here we will focus on the infrared spectrum recorded at the temperature of 49 K [15, 59]. We have performed rovibrational calculations for the  $V_{nT(Q)}$  surface with the BOUND package [60], using the coupled-channel method. The details of these calculations are the same as in Refs. [15, 30]. Because the considered van der Waals spectrum accompanies the fundamental band of CO, we had to perform the rovibrational calculations for both  $v_2 = 0$  and  $v_2 = 1$  versions of  $V_{nT(Q)}$ .

The rovibrational wave functions of the H<sub>2</sub>-CO complex can be characterized, for given vibrational states of H<sub>2</sub> and CO, by two exact quantum numbers: the total angular momentum J and the spectroscopic parity defined as  $P = (-1)^{J+j_1+j_2+l}$ where  $j_1$  and  $j_2$  are the quantum numbers of the angular momenta of  $H_2$  and CO, respectively, and l denotes the quantum number of the end-over-end rotation of the complex (i.e., for a given P and J, the sum of  $j_1 + j_2 + l$  has to be odd or even for all  $j_1$ ,  $j_2$ , and l appearing in the basis set used to expand the rovibrational wave function). To denote the P = +1 and -1 parities, we will use notation P = e or f, respectively. There are several rovibrational states in each block numbered by Jand P. To distinguish between them, one can use approximate quantum numbers. In Ref. [59], McKellar proposed to use  $(J, P, j_2, l)$  to characterize the states of  $paraH_2$ CO. To extend such labeling to the  $orthoH_2$ -CO complex, one needs to use also the  $j_{12}$ approximate quantum number, denoting the coupling of  $j_1$  and  $j_2$ . Thus, altogether one can use  $(J, P, j_1, j_2, j_{12}, l)$ , where  $j_1, j_2, j_{12}$ , and l are approximate quantum numbers. This labeling was used, for example, in Refs. [15, 61, 62], but it leads to ambiguities. Therefore, in the present paper we will use  $n_{J,P}$ , the number of the consecutive-energy state in each J, P block.

It has been shown in Refs. [15, 30] that to obtain theoretical infrared spectra of the  $H_2$ –CO complex that resemble experimental ones, one has to consider quasi-bound states. To obtain these low-energy resonances, we have used the stabilization method and the BOUND program. In the case of  $paraH_2$ –CO, the dissociation limit is 0 for the states of the P = e symmetry and  $2 \cdot B(CO(v_2 = 0)) = 3.845$  cm<sup>-1</sup> for P = f. This defines the threshold energies above which the states are the resonances.

In Table 2, the rovibrational energies for  $paraH_2$ -CO calculated from  $V_{nT(O)}$  and  $V_{12}$  are compared to each other and to the experimental values. Let us first discuss the dissociation energies listed in the captions. The values calculated with  $V_{\rm nT(Q)}$  differ by about  $0.7 \text{ cm}^{-1}$  from  $V_{12}$  ones, consistent with the change of the depth of the  $V_{\rm nT(Q)}$ surface relative to  $V_{12}$ . The comparison of  $\Delta^v_{\mathrm{nT(Q)}}$  with  $\Delta^v_{12}$  shows that the deviation of the  $E_{\rm nT(O)}^v$  energies from their experimental counterparts are much larger than in the case of  $E_{12}^{v'}$ . The values of the root mean square error, RMSE, of  $E_{nT(Q)}^{v}$  relative to the experimental values, are equal to  $0.072 \text{ cm}^{-1}$  for both  $v_2 = 0$  and  $v_2 = 1$  cases, whereas the corresponding RMSEs of  $E_{12}^v$  amount to 0.005 cm<sup>-1</sup> and 0.007 cm<sup>-1</sup>, an order of magnitude difference. From Table 2, one can also notice that for some rovibrational states the values of  $\Delta^{v}_{nT(Q)}$  are relatively small, while for others the discrepancies are quite substantial. This can be attributed to the change of anisotropy of  $V_{\rm nT(Q)}$  relative to  $V_{12}$  discussed in Sec. 2. Since the energies  $E_{\rm nT(Q)}^v$  are given relative to the ground state energy, the position of the excited states probing similar parts of the interaction energy surface as the ground state should be affected in a similar way as the ground state, leading to small discrepancies, in contrast to the excited states probing different parts of the surface than the ground state does. The largest values of the difference  $\Delta_{12,\mathrm{nT(Q)}}^v = E_{\mathrm{nT(Q)}}^v - E_{12}^v$  are about 0.18 cm<sup>-1</sup>, large comparing to the resolution of the experiment, but consistent with the change of anisotropy caused by the  $\delta E_{\rm int}^{\rm T(Q)}$ term.

The rovibrational energy pattern for orthoH<sub>2</sub>-CO is much richer than in the case of paraH<sub>2</sub>-CO and there are about three times more rovibrational states, both bound and quasibound. The complete list of the energy levels for orthoH<sub>2</sub>-CO calculated for  $v_2 = 0$  and  $v_2 = 1$  with  $V_{\rm nT(Q)}$  is given in Table 3. These energies are compared with their counterparts calculated with  $V_{12}$ . The calculated energies are all positive because the dissociation limit for the  $j_1 = 1$  rotational state of H<sub>2</sub> is at 118.644 cm<sup>-1</sup> and the energy zero is defined for  $H_2(v_1=0,j_1=0)$  and  $CO(v_2=0 \text{ or } v_2=1,j_2=0)$ separated to infinity. Unlike the  $paraH_2$ -CO case, only for the  $J^P = 0^f$  symmetry block the dissociation limit is higher by  $2 \cdot B(CO(v_2 = 0)) = 3.845 \text{ cm}^{-1}$ , because  $j_2$ cannot be equal to 0 due to the definition of the f symmetry and the rules of coupling of angular momenta. For  $V_{\rm nT(Q)}$  ( $V_{12}$ ), the ground-state energies, listed in captions of  $v_2 = 0$  and  $v_2 = 1$ , respectively, and the energies  $E_{nT(Q)}^v$  ( $E_{12}^v$ ) are given relative to them. From the ground-state energies, one can calculate the  $V_{\rm nT(Q)}$  ( $V_{12}$ ) dissociation energies that are equal to  $19.913 \text{ cm}^{-1} (20.677 \text{ cm}^{-1})$  and  $20.114 \text{ cm}^{-1} (20.855 \text{ cm}^{-1})$ for  $v_2 = 0$  and 1, respectively. The  $V_{\rm nT(Q)}$  ones are smaller than  $V_{12}$  counterparts by  $0.764 \text{ cm}^{-1}$  and  $0.741 \text{ cm}^{-1}$  for the two values of v. These shifts of the dissociation energies are similar to those in the interaction energies and are mainly caused by the smaller depth of  $V_{nT(Q)}$  in comparison with  $V_{12}$ .

Similarly to the rovibrational energy levels of  $paraH_2$ –CO, the discrepancies of the energies calculated from  $V_{\rm nT(Q)}$  and  $V_{12}$ , measured by  $\Delta^v_{12,\rm nT(Q)} = E^v_{\rm nT(Q)} - E^v_{12}$ , vary significantly from state to state, and are as large as 0.7 cm<sup>-1</sup> in some cases. This

particular value is larger by  $0.2 \text{ cm}^{-1}$  than for  $paraH_2$ –CO. This difference can be explained by the different nature of the  $H_2$ -related component in the rovibrational wave functions of the two complexes. In the case of  $paraH_2$ –CO, the  $j_1 = 0$  component dominates the wave function, whereas in the case of  $orthoH_2$ –CO, it is  $j_1 = 1$ . Thus, the rovibrational wave function of  $orthoH_2$ –CO is more sensitive to changes of anisotropy of the surface because in the case of  $paraH_2$ –CO the changes in anisotropy are averaged over the orientations of the  $H_2$  molecule. The deviation of the  $E^v_{nT(Q)}$  energies from the  $E^v_{12}$  ones, measured by RMSE, is equal to  $0.122 \text{ cm}^{-1}$  for both values of  $v_2$ , and is larger than the corresponding deviations for  $paraH_2$ –CO. This difference can be once more attributed to the nature of the rovibrational wave function that in the case of  $orthoH_2$ –CO probes the anisotropy of the interaction energy surface more strongly. For  $paraH_2$ –CO, we were able to make comparisons to experimental energy levels. Unfortunately, such levels are not available for  $orthoH_2$ –CO. Instead, we will compare directly spectral lines.

From Tables 2 and 3, one can see that there are less bound states obtained from the  $V_{\rm nT(Q)}$  surface than from the  $V_{12}$  one. This is due to the fact that the  $V_{\rm nT(Q)}$  surfaces, for both values of  $v_2$ , are shallower than their  $V_{12}$  counterparts, and the dissociation energies calculated from  $V_{\rm nT(Q)}$  are smaller than the corresponding energies obtained from  $V_{\rm nT(Q)}$ . Consequently, some bound states that are just below the dissociation limit in the case of the  $V_{12}$  calculations, pop out of the potential well in the case of the  $V_{\rm nT(Q)}$  surface and form quasi-bound states.

From the considerations above, we already know that the rovibrational energy levels obtained from  $V_{\rm nT(Q)}$ , are significantly different from their counterparts obtained using  $V_{12}$ , both for para and orthoH<sub>2</sub>–CO. The next question is, how much those differences affect the spectra. To find this out, we have computed the ab initio infrared spectra at 49 K to compare them with the experimental ones recorded by McKellar [15, 59]. The calculations were performed in the way described in Refs. [15, 30]. The resulting  $V_{\rm nT(Q)}$  spectra and their comparison to the experimental and  $V_{12}$  ones, are presented in the Supplementary Materials (SM) in Figs. S1 and S2, for the para and orthoH<sub>2</sub>–CO cases, respectively. Also in SM, we included tables listing all theoretical transitions with relative intensities larger than 0.01. The selected fragments of the whole spectra are presented in Fig. 2 for paraH<sub>2</sub>–CO and Fig. 3 for orthoH<sub>2</sub>–CO.

One could potentially compare directly the spectra computed from  $V_{\rm nT(Q)}$  and  $V_{12}$  with experimental spectra to obtain quantitative measures of the discrepancies. However, in the former case, the correspondence between the lines is far from unique for a few percent of lines, and it would be even difficult to define an algorithm for relating the lines (see below). Thus, we present here only qualitative analysis of the differences between theoretical and experimental spectra.

First, let us focus on the  $paraH_2$ –CO spectrum presented in Fig. 2. There are some fragments of spectrum, e.g., those indicated by the green shading, where the peaks obtained from  $V_{\rm nT(Q)}$  can be easily correlated with the experimental ones. Although some of the peaks are significantly shifted, like in cells II and VII, they are well separated and the theoretical patterns agree pretty well with the experimental ones. However, one can see that the  $V_{12}$  spectrum is still closer to experiment. There are also fragments of the spectrum, shaded in blue, where the agreement of the  $V_{\rm nT(Q)}$  lines with the experimental ones appears to be good, but there are distortions which can cause problems in the assignment of experimental lines. For instance, in cell I, the calculated transition denoted by A is shifted so much that one could ignore it and try to correlate the theoretical very small peak at 2.9 cm<sup>-1</sup> with the peak A

in the experimental spectrum. In cell VI, one can see a similar example, where the transition A calculated from  $V_{\rm nT(Q)}$  is so close to the transition D that both of them could be correlated with the transition D in the experimental spectrum. In the case of the  $V_{12}$  spectrum, the A transition is very close to B, and both of them can be correlated with one line in the experimental spectrum. The most problematic parts of the  $V_{\rm nT(Q)}$  spectrum are those indicated with magenta. In cell V, there are three well-separated transitions with similar intensities. If one knew only the  $V_{\rm nT(Q)}$  peaks and the experimental ones, it would be almost impossible to make the proper assignments. In this case, the quantitative disagreement turns into the qualitative one. In another case, shown in cell III, there are three lines with C significantly shifted in  $V_{\rm nT(Q)}$ , which causes the wrong order of the lines. Although from the intensities of the lines one can guess the correct order and make the proper assignment, some doubts would remain. It should be emphasized that in all discussed cells of the spectrum, the transitions calculated with  $V_{12}$  are very close to those recorded in the experiment.

In the case of the orthoH<sub>2</sub>-CO spectrum, presented in Fig. 3, one can also distinguish some parts of the spectrum with different levels of agreement between the  $V_{\rm nT(O)}$ theoretical transitions and the experimental ones. In cell I, there are five experimental peaks nicely modeled by the  $V_{12}$  spectrum. However, in the  $V_{\rm nT(Q)}$  spectrum, the transitions marked by A is shifted more than the other ones and, as a consequence, although the resulting pattern of the lines resembles, to some extent, the experimental one, it would be difficult to make proper assignments only on the base of the  $V_{\rm nT(O)}$ calculations. In the case of cell II, the pattern of lines obtained from  $V_{\rm nT(Q)}$  is totally different from that obtained from  $V_{12}$ . Whereas the latter one can be correlated with the experimental lines with relatively high confidence, a similar outcome could not be expected for the former one. Another pattern of lines with improper order is shown in cell IV. If one uses the positions of the  $V_{\rm nT(Q)}$  lines to assign the experimental spectrum, the B and C lines would be missassigned. One can make assignment also from comparisons of the intensities, but it would be difficult to choose which contradictory criterion should be used for the assignment: the positions or the intensities. In the fields indicated by the blue shading, one can find cases for which the  $V_{\rm nT(Q)}$  calculations can lead to less certain assignments of the experiment. In cell VI, the positions of the  $V_{\rm nT(Q)}$  peaks are shifted with respect to the experimental ones, and B and C on the  $V_{\rm nT(Q)}$  side resemble peaks A and B on the experimental side, while the weak feature at -2.8 cm  $^{-1}$  of the  $V_{\rm nT(Q)}$  could be wrongly connected with the experimental C transition. In this case, the agreement of the  $V_{12}$  peaks with the experimental ones, although not ideal, is good enough to give the correct assignment. In the case of cell V, two well-separated peaks obtained from the  $V_{\rm nT(Q)}$  calculations can be hardly recognized as the contributors to one strong line in the experimental spectrum. However, one should emphasize that there are also the fragments calculated from  $V_{\rm nT(Q)}$  that are very close to the experimental ones, e.g., cell VII in Fig. 3.

The comparisons of the theoretical spectrum calculated from  $V_{\rm nT(Q)}$  with the experimental one discussed above show that in some cases the accuracy of the  $V_{\rm nT(Q)}$  spectrum is not sufficiently high to perform an unambiguous assignment of the experimental spectrum. This is the case even for the  $paraH_2$ –CO complex, where the spectrum is relatively sparse.

#### 4. Conclusions

The effects of full triple and iterative quadruple excitations on ab initio predictions of properties of molecular clusters have been investigated on the example of H<sub>2</sub>-CO by comparing rovibrational spectra of this complex computed with the T(Q) contributions included or neglected to the measured spectra. The interaction energies have been computed on a six-dimensional grid applying a base level of theory: CCSD(T) in up to augmented quadruple-zeta quality basis sets. These calculations were used to develop a Taylor expansion of the interaction energy in powers of the intramonomer coordinates for each point of the intermonomer grid. Then the leading term of this expansion was replaced by the interaction energies computed at higher levels of theory. Two such level were included: one with CCSD(T) in up to augmented quintuple-zeta quality basis sets and another one with T(Q) contributions computed in augmented doublezeta quality bases added to the former results. Both 6D surfaces were then averaged over the intramonomer coordinates giving 4D surfaces denoted as  $V_{\rm nT(Q)}$  and  $V_{12}$ , respectively. The latter surface was actually developed earlier in Ref. [15] and was used here without any changes. Also the spectra computed from  $V_{12}$  were taken from that reference. The spectra from  $V_{\rm nT(Q)}$  were computed in the present work.

The effects of the T(Q) contribution on interaction energies were already discussed in Ref. [15]. We extended this discussion here by plotting these effects as functions of the angular coordinates to examine their anisotropy. We found that the addition of the T(Q) contribution increases the anisotropy ration on the path from the minimum at  $\theta_2 = 180^{\circ}$  to  $\theta_2 = 0^{\circ}$  from 1.64 to 1.68. While these ratios may seem to be similar to each other, their difference corresponds to 2.4 cm<sup>-1</sup>, which is a significant difference at the level of theory applied here, which results in discrepancies with experimental spectra sometimes as small as 0.001 cm<sup>-1</sup>.

The main goal of our work was, however, the comparison with experimental spectra. For the  $paraH_2$ –CO, the experimental energy levels are available and we could make very precise quantitative comparisons. The RMSE of  $V_{nT(Q)}$  ( $V_{12}$ )-level theory relative to experiment was found to be 0.072 (0.005) and 0.072 (0.007) cm<sup>-1</sup> for the CO ground and first excited vibrational states, respectively. Thus, the addition of the T(Q) contributions leads to a dramatic improvement of agreement between theory and experiment. Apparently, the fact that the uncertainties of the T(Q) terms due to the basis set size, estimated in Ref. [55], can be as large as 35%, does not impair this improvement. We believe the main reason for the behaviour observed is that the significant anisotropy of the T(Q) contribution apparently leads to improved anisotropy of the whole surface. Were this contribution more isotropic, it would result in a uniform lowering of such surface. Such a lowering has only a small impact on energy levels since they are given relative to the energy of the lowest rovibrational state. Of course, the latter energy, which is equal to the negative of the dissociation energy, is affected by the T(Q) contribution independent of its anisotropy.

For  $ortho \rm H_2$ –CO, experimental energy levels are unknown and therefore an analogous analysis cannot be made. One could calculate RMSEs of theoretical lines with respect to experimental ones, but as discussed earlier, this procedure would be highly nonunique in the case of  $V_{\rm nT(Q)}$ . Therefore, we discuss the relative performance only in qualitative terms (for both spin species). It is found that while the spectra generated from  $V_{12}$  agree qualitatively (in fact, also quantitatively) with experiment virtually in the whole measured range, the spectra generated from  $V_{\rm nT(Q)}$  are not in qualitative agreement with experiment is several regions of the spectrum with lines appearing in different orders.

PESs computed by fitting to ab initio data can be used to generate spectra and then improved by adjusting some parameters of the fit to increase the agreement of the computed and measured spectra. Such procedures, called tunning or morphing, have been used since 1990s, see, e.g., Refs. [5, 63, 64]. One may ask how accurate the initial surface should be to make such tuning successful. Our results show that the expectations that even a low-accuracy first-principles PES will be sufficient provided it has minima and saddle point at proper geometries is not correct. In the case  $V_{\rm nT(Q)}$ , the positions and depths of the minima are very similar to those of  $V_{12}$ , while the infrared spectra obtained from  $V_{\rm nT(Q)}$  are so different from the experimental ones that they could lead to the wrong initial assignment of the spectral lines, to which the morphed surface is fitted. Thus, in the case of  $H_2$ -CO, one could successfully perform the tuning procedure based on the  $V_{12}$  theoretical spectrum, but not starting from the  $V_{\rm nT(Q)}$  spectrum. In general, the condition that the first-principles PES has to satisfy is that it correctly assigns the spectrum.

# Acknowledgments

This research was supported by the National Science Centre, Poland, Grant No. 2017/25/B/ST4/01300 [P.J. and E.G.] and by the National Science Foundation under Grant No. CHE-1900551 [K.Sz.].

# References

- [1] J.M. Hutson, Annu. Rev. Phys. Chem. 41, 123–154 (1990).
- A. van der Avoird, P.E.S. Wormer and R. Moszyński, Chem. Rev. 94, 1931–1974 (1994).
- [3] V.F. Lotrich, H.L. Williams, K. Szalewicz, B. Jeziorski, R. Moszynski, P.E.S. Wormer and A. van der Avoird, J. Chem. Phys. 103, 6076–6092 (1995).
- W. Klopper, M. Quack and M.A. Suhm, J. Chem. Phys. 108, 10096-10115 (1998).
- [5] M. Meuwly and J.M. Hutson, J. Chem. Phys. 110, 8338–8347 (1999).
- [6] A.J. Misquitta, R. Bukowski and K. Szalewicz, J. Chem. Phys. 112, 5308-5319 (2000).
- [7] P.E.S. Wormer and A. van der Avoird, Chem. Rev. **100**, 4109–4143 (2000).
- [8] K. Müller-Dethlefs and P. Hobza, Chem. Rev. 100, 143–167 (2000).
- [9] R. Bukowski, K. Szalewicz, G.C. Groenenboom and A. van der Avoird, J. Chem. Phys. 128, 094314 (2008).
- [10] W. Cencek, K. Szalewicz, C. Leforestier, R. van Harrevelt and A. van der Avoird, Phys. Chem. Chem. Phys. 10, 4716–4731 (2008).
- [11] A. van der Avoird and K. Szalewicz, J. Chem. Phys. 128, 014302 (2008).
- [12] K. Szalewicz, Int. Rev. Phys. Chem. 27, 273–316 (2008).
- [13] X. Huang, B.J. Braams, J.M. Bowman, R.E.A. Kelly, J. Tennyson, G.C. Groenenboom and A. van der Avoird, J. Chem. Phys. 128, 034312 (2008).
- [14] B.J. Braams and J.M. Bowman, Intern. Rev. Phys. Chem. 28, 577–606 (2009).
- [15] P. Jankowski, A.R.W. McKellar and K. Szalewicz, Science 336, 1147–1150 (2012).
- [16] C. Leforestier, K. Szalewicz and A. van der Avoird, J. Chem. Phys. 137, 014305 (2012).
- [17] R. Dawes, X. Wang and T. Carrington, Jr., J. Phys. Chem. A 117, 7612-7630 (2013).
- [18] J. Brown, X.G. Wang, T. Carrington, Jr., G.S. Grubbs, II and R. Dawes, J. Chem. Phys. 140, 114303 (2014).
- [19] V. Babin, C. Leforestier and F. Paesani, J. Chem. Theory Comput. 9, 5395–5403 (2013).
- [20] M.P. Metz, K. Szalewicz, J. Sarka, R. Tóbiás, A. Császár and E. Matyus, Phys. Chem. Chem. Phys. 21, 13505–13525 (2019).

- [21] R. Dawes and E. Quintas-Sanchez, in Rev. Comp. Chem., edited by A. L. Parrill and K.B. Lipkowitz, Vol. 31 (Wiley, 2019), pp. 199–263.
- [22] J. Huang, D. Yang, Y. Zhou and D. Xie, J. Chem. Phys. 150, 154302 (2019).
- [23] X. Wang and T. Carrington, Jr., J. Chem. Phys. 148, 074108 (2018).
- [24] G. Avila, D. Papp, G. Czako and E. Matyus, Phys. Chem. Chem. Phys. 22, 2792–2802 (2020).
- [25] M. Urban, J. Noga, S.J. Cole and R.J. Bartlett, J. Chem. Phys. 83, 4041–4046 (1985).
- [26] K. Raghavachari, G.W. Trucks, J.A. Pople and M. Head-Gordon, Chem. Phys. Lett. 157, 479 (1989).
- [27] R.J. Bartlett and J.F. Stanton, Rev. Comp. Chem. 5, 65–169 (1994).
- [28] R.J. Bartlett, in Modern Electronic Structure Theory, edited by D. R. Yarkony (World Scientific, Singapore, 1995), pp. 1047–1131.
- [29] J.F. Stanton, Chem. Phys. Lett. **281**, 130–134 (1997).
- [30] P. Jankowski, L.A. Surin, A.V. Potapov, S. Schlemmer, A.R.W. McKellar and K. Szalewicz, J. Chem. Phys. 138, 084307 (2013).
- [31] J.R. Lane, J. Chem. Theory Comput. 9, 316–323 (2013).
- [32] A.D. Boese, J. Chem. Theory Comput. 9, 4403–4413 (2013).
- [33] J.F. Stanton and R.J. Bartlett, J. Chem. Phys. 98, 7029–7039 (1993).
- [34] J. Noga and R.J. Bartlett, J. Chem. Phys. 86, 7041–7050 (1987).
- [35] J.D. Watts, J. Gauss and R.J. Bartlett, J. Chem. Phys. 98, 8718–8733 (1993).
- [36] Y.J. Bomble, J.F. Stanton, M. Kállay and J. Gauss, J. Chem. Phys. 123, 054101 (2005).
- [37] J.F. Stanton, C. Lopreore and J. Gauss, J. Chem. Phys. 108, 7190-7196 (1998).
- [38] K.L. Bak, J. Gauss, P. Jorgensen, J. Olsen, T. Helgaker and J.F. Stanton, J. Chem. Phys. 114, 6548–6556 (2001).
- [39] F. Pawlowski, P. Jørgensen, J. Olsen, F. Hegelund, T. Helgaker, J. Gauss, K.L. Bak and J.F. Stanton, J. Chem. Phys. 116, 6482–6496 (2002).
- [40] C. Puzzarini, J.F. Stanton and J. Gauss, Int. Rev. Phys. Chem. 29, 273–267 (2010).
- [41] Z.N. Heim, B.K. Amberger, B.J. Esselman, J.F. Stanton, R.C. Woods and R.J. McMahon, J. Chem. Phys. 152, 104303 (2020).
- [42] K. Sharma, T.A. Miller and J.F. Stanton, Int. Rev. Phys. Chem. 40, 165–298 (2021).
- [43] A. Tajti, P.G. Szalay, A.G. Császár, M. Kállay, J. Gauss, E.F. Valeev, B.A. Flowers, J. Vázquez and J.F. Stanton, J. Chem. Phys. 121, 11599–11613 (2004).
- [44] Y.J. Bomble, J. Vázquez, M. Kállay, C. Michauk, P.G. Szalay, A.G. Császár, J. Gauss and J.F. Stanton, J. Chem. Phys. 125, 064108 (2006).
- [45] M. Kodrycka and K. Patkowski, J. Chem. Phys. **151**, 070901 (2019).
- [46] G.S. Tschumper, M.L. Leininger, B.C. Hoffman, E.F. Valeev, H.F. Schaefer III and M. Quack, J. Chem. Phys. 116, 690–701 (2002).
- [47] J. Řezáč, L. Šimová and P. Hobza, J. Chem. Theory Comput. 9, 364–369 (2013).
- [48] J. Řezáč and P. Hobza, J. Chem. Theory Comput. 9, 2151–2155 (2013).
- [49] L. Demovičova, P. Hobza and J. Řezáč, Phys. Chem. Chem. Phys. 16, 19115–19121 (2014).
- [50] J. Řezáč and P. Hobza, J. Chem. Theory Comput. 10, 3066–3073 (2014).
- [51] K. Patkowski, W. Cencek, P. Jankowski, K. Szalewicz, J.B. Mehl, G. Garberoglio and A.H. Harvey, J. Chem. Phys. 129, 094304 (2008).
- [52] G. Garberoglio, P. Jankowski, K. Szalewicz and A.H. Harvey, J. Chem. Phys. 137, 154308 (2012).
- [53] B.W. Bakr, D.G.A. Smith and K. Patkowski, J. Chem. Phys. 139, 144305 (2013).
- [54] F. Thibault, K. Patkowski, P.S. Żuchowski, H. Jóźwiak, R. Ciuryło and P. Wcisło, J. Quant. Spectr. Rad. Trans. 202, 308–320 (2017).
- [55] D.G.A. Smith, P. Jankowski, M. Slawik, H.A. Witek and K. Patkowski, J. Chem. Theory Comput. 10, 3140–3150 (2014).
- [56] G. Garberoglio, P. Jankowski, K. Szalewicz and A.H. Harvey, J. Chem. Phys. 146, 054304 (2017).
- [57] R.A. Kendall, T.H. Dunning, Jr. and R.J. Harrison, J. Chem Phys. 96, 6796–6806 (1992).
- [58] A. Halkier, W. Klopper, T. Helgaker, P. Jørgensen and P.R. Taylor, J. Chem. Phys. 111,

- 9157-9167 (1999).
- [59] A.R.W. McKellar, J. Chem. Phys. 108, 1811–1820 (1998).
- [60] J.M. Hutson and C.R. Le Sueur MOLSCAT, BOUND, and FIELD, version 2020.0, https://github.com/molscat/molscat (2020).
- [61] P. Jankowski and K. Szalewicz, J. Chem. Phys. 108, 3554–3565 (1998).
- [62] P. Jankowski and K. Szalewicz, J. Chem. Phys. 123, 104301 (2005).
- [63] E.H.T. Olthof, A. van der Avoird and P.E.S. Wormer, J. Chem. Phys. 101, 8430–8442 (1994).
- [64] E.M. Mas, R. Bukowski, K.S.G.C. Groenenboom, P.E.S. Wormer and A. van der Avoird, J. Chem. Phys. 113, 6687–6701 (2000).

**Table 1.** The positions  $(R_{\min})$  and values  $(E_{\min})$  of the global and local minima on the  $V_{\rm nT(Q)}$  and  $V_{12}$  surfaces. The values for  $V_{12}$  are taken from Ref. [30]. The distances are given in bohr and energies in cm<sup>-1</sup>. The angle  $\phi = 0^{\circ}$ .

	$(\theta_1, \theta_2)$ =	$=(0^{\circ},180^{\circ})$	$(\theta_1, \theta_2)$	$=(0^{\circ},0^{\circ})$
	$R_{\min}$	$E_{ m min}$	$R'_{\min}$	$E'_{\min}$
		$v_2 =$	= 0	
$\overline{V_{\mathrm{nT(Q)}}}$	7.931	-91.266	7.176	-72.981
$V_{12}$	7.911	-94.096	7.168	-73.738
		$v_2 =$	: 1	
$V_{\rm nT(Q)}$	7.946	-89.976	7.176	-73.996
$V_{12}$	7.925	-92.775	7.169	-74.769

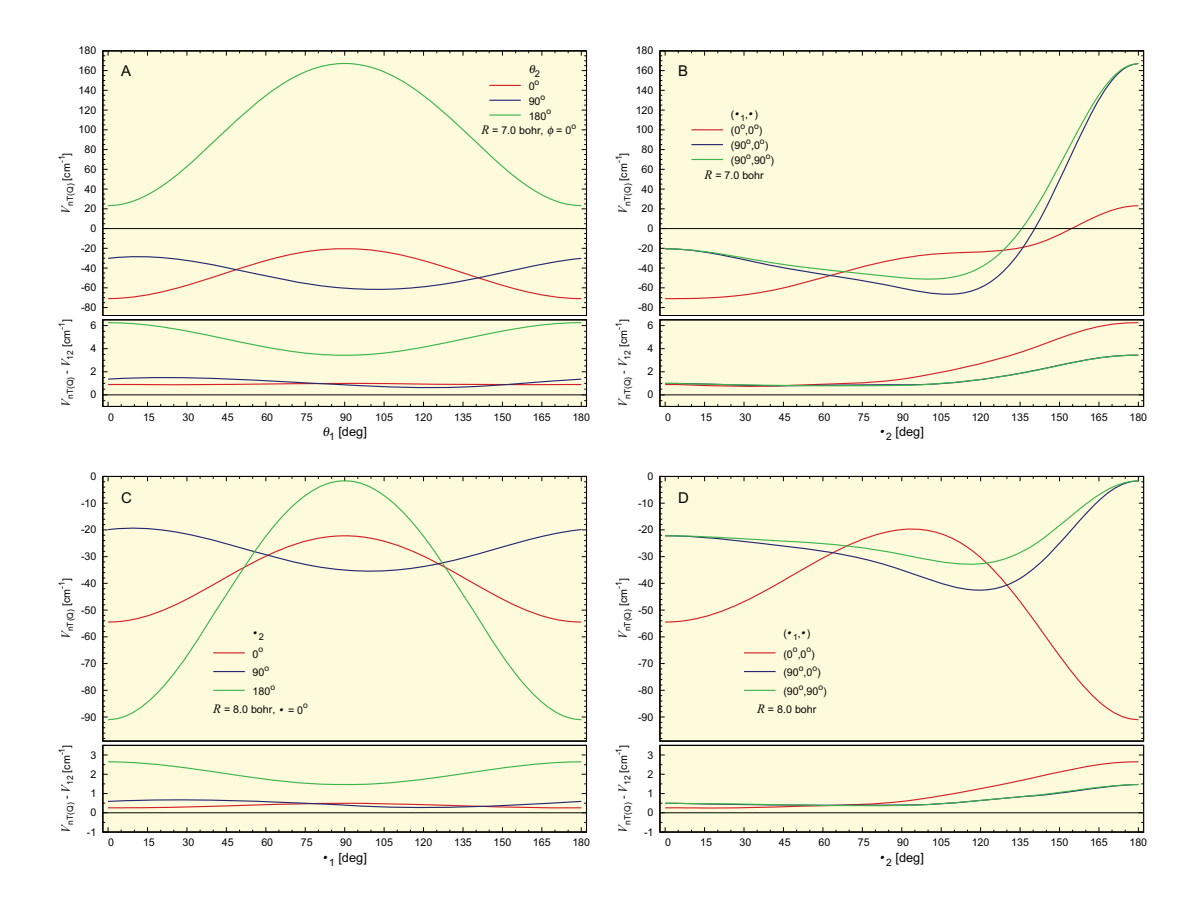


Figure 1. Comparison of the  $V_{\rm nT(Q)}$  and  $V_{12}$  interaction energy surfaces for several geometries with the  $\theta_1$  or  $\theta_2$  angles varying and other intermolecular coordinates constant. In the upper part of each panel, there are plots of the  $V_{\rm nT(Q)}$  surface, while the corresponding differences between two surfaces,  $V_{\rm nT(Q)} - V_{12}$ , are plotted in the lower part of each panel.

Table 2. Comparison of the rovibrational energies  $E^v_{\rm nT(Q)}$  and  $E^v_{12}$ , for  $para\rm H_2\text{-CO}$  calculated with the  $V_{\rm nT(Q)}$  and  $V_{12}$  surfaces, with the experimental values  $E^v_{\rm expt}$  [59]. The theory-experiment discrepancies  $\Delta^v_{\rm nT(Q)} = E^v_{\rm nT(Q)} - E^v_{\rm expt}$  and  $\Delta^v_{12} = E^v_{12} - E^v_{\rm expt}$  are also listed. The differences between the theoretical energies are denoted by  $\Delta^v_{12,\rm nT(Q)} = E^v_{\rm nT(Q)} - E^v_{12}$ . The values of  $E^v_{\rm nT(Q)}$  and  $E^v_{12}$  are given relative to the energies of the ground states, which amount to -18.705 (-19.440) cm<sup>-1</sup> and -18.884 (-19.616) cm<sup>-1</sup> for v=0 and 1, respectively, for  $E^v_{\rm nT(Q)}$  ( $E^v_{12}$ ). Note that the zero of energy is for  $H_2(v_1=0,j_1=0)$  and  $CO(v_2=0$  or  $v_2=1,j_2=0$ ) separated to infinity. The resonance states are denoted with asterisks. RMSEs are calculated for all rovibrational energy levels presented in the table. The results for  $V_{12}$  are taken from Ref. [15]. The unit of energy is cm<sup>-1</sup>.

$\overline{J}$	$\overline{P}$	$n_{J,P}$	$E_{\text{expt}}^0$	$E_{12}^{0}$	$\Delta^0_{12}$	$E_{\rm nT(Q)}^0$	$\Delta_{\mathrm{nT(Q)}}^{0}$	$\Delta^{0}_{12,nT(Q)}$	$E_{\rm expt}^1$	$E_{12}^{1}$	$\Delta^1_{12}$	$E^1_{\rm nT(Q)}$	$\Delta_{\rm nT(Q)}^1$	$\Delta^1_{12,nT(Q)}$
0	2	1	0.000	0.000	0.000	$\frac{{\rm nT(Q)}}{0.000}$	$\frac{-nT(Q)}{0.000}$	0.000	0.000	0.000	0.000	$\frac{-\text{nT(Q)}}{0.000}$	$\frac{-\text{nT(Q)}}{0.000}$	0.000
0	2	2	7.079	7.083	0.004	7.045	-0.034	-0.038	7.056	7.052	-0.004	7.015	-0.041	-0.037
0	2	3	15.168			15.083	-0.085	-0.095		15.122		15.033	-0.088	-0.089
1	1	1	4.090	4.085	-0.005	4.115	0.025	0.030	4.067	4.059	-0.008	4.090	0.023	0.031
1	1	2	15.665	15.654	-0.011	15.624	-0.041	-0.030	15.570	15.555	-0.015	15.526	-0.044	-0.029
1	2	1	1.054	1.055	0.001	1.047	-0.007	-0.008	1.059	1.055	-0.004	1.047	-0.012	-0.008
1	2	2	3.618	3.614	-0.004	3.645	0.027	0.031	3.596	3.587	-0.009	3.620	0.024	0.033
1	$\frac{2}{2}$	3	8.485 13.660	8.489	0.004	8.443	-0.042	-0.046 -0.032	8.463	8.460 $13.573$	-0.003	8.415	-0.048	-0.045 -0.029
1	2		17.913			13.626 $17.738$	-0.034 -0.175	-0.032 -0.176		17.866		13.544 17.710	-0.039 -0.162	-0.029
1	2	9	17.913	17.914	0.001	11.130	-0.175	-0.170	11.012	17.000	-0.000	17.710	-0.102	-0.150
2	1	1	6.266	6.263	-0.003	6.278	0.012	0.015	6.246	6.238	-0.008	6.254	0.008	0.016
2	1	2	11.690	11.686		11.725	0.035	0.039	11.600	11.592	-0.008	11.632	0.032	0.040
2	1	3	18.341	18.332	-0.009	18.283	-0.058	-0.049	18.252	18.239	-0.013	18.191	-0.061	-0.048
2	2	1	3.148	3.150	0.002	3.125	-0.023	-0.025	3.153	3.151	-0.002	3.126	-0.027	-0.025
2	2	2	5.014	5.011	-0.003	5.033	0.019	0.022	4.994	4.985	-0.009	5.009	0.015	0.024
2	2		11.097		0.009	11.045	-0.052	-0.061	11.059	11.063		11.009	-0.050	-0.054
2	2	4		11.357		11.386	0.019	0.029	11.296			11.306	0.010	0.025
2	2	5	14.807	14.807	0.000	14.776	-0.031	-0.031	14.731	14.726	-0.005	14.697	-0.034	-0.029
3	1	1	9.490	9.489	-0.001	9.481	-0.009	-0.008	9.473	9.468	-0.005	9.461	-0.012	-0.007
3	1		14.079			14.094	0.015	0.018		13.982		14.002	0.012	0.020
3	1	3		22.104		22.018	-0.093	-0.086		22.018		21.936	-0.093	-0.082
3	1	4	23.164			23.195*	0.031	0.034		22.965		23.001*	0.029	0.036
3	2	1	6.248	6.253	0.005	6.199	-0.049	-0.054	6.254	6.255	0.001	6.200	-0.054	-0.055
3	2	2	7.293	7.289	-0.004	7.300	0.007	0.011	7.277	7.268	-0.009	7.282	0.005	0.014
3	2		12.933			12.939	0.006	0.006		12.839		12.847	0.002	0.008
3	2		14.821			14.729	-0.092	-0.093	14.811			14.715	-0.096	-0.092
3	2	5	17.501	17.506	0.005	17.461	-0.040	-0.045	17.427	17.426	-0.001	17.385	-0.042	-0.041
4	1	1	13.709	19 711	0.002	13.669	-0.040	-0.042	13.698	12 605	0.002	13.656	-0.042	-0.039
4	1		17.403			17.391	-0.040	-0.042	17.317			17.301	-0.042	-0.039
4	1	4	11.400	11.402	-0.001	11.001	-0.012	-0.011	11.011	17.511	-0.000	11.501	-0.010	-0.010
4	2	1	10.272	10.285	0.013	10.172	-0.100	-0.113	10.260	10.269	0.009	10.156	-0.104	-0.113
4	2	2		10.509		10.523	0.006	0.014		10.513		10.529	0.002	0.016
4	2		15.255			15.234	-0.021	-0.021		15.166		15.146	-0.025	-0.020
4	2	4	19.411	19.414	0.003	19.271*	-0.140	-0.143	19.411	19.407	-0.004	19.268*	-0.143	-0.139
5	1		18.831			18.750	-0.081	-0.087		18.829		18.745	-0.084	-0.084
5	1	2	21.650	21.651	0.001	21.598	-0.052	-0.053	21.567	21.563	-0.004	21.513	-0.054	-0.050
E	0	1	14 504	14 597	0.009	1 / / / / / / /	0.079	0.076	14 510	14 500	0.000	14 491	0.070	0.077
5 5	$\frac{2}{2}$		14.524 $15.273$			14.451 $15.180$	-0.073 -0.093	-0.076 -0.099	14.510	14.508 $15.297$		14.431 $15.205$	-0.079 -0.092	-0.077 -0.092
5	2		18.426			18.368	-0.058	-0.099		18.343		18.286	-0.092	-0.092
J	4	J	10.420	10.420	0.002	10.000	-0.000	-0.000	10.041	10.040	-0.004	10.200	-0.001	-0.001
6	1	1	24.683	24.692*	0.009	24.535*	-0.148	-0.157	24.695	24.699*	0.004	24.547*	-0.148	-0.152
6	1			26.773*		26.659*	-0.109	-0.114		26.693*		26.582*	-0.110	-0.111
													, and the second	
6	2		19.401			19.296*	-0.105	-0.106		19.398	-0.004	19.293*	-0.109	-0.105
6	2			$20.939^*$		20.766*	-0.163	-0.173		$20.960^{*}$		$20.797^*$	-0.159	-0.163
6	2	3	22.468	22.466*	-0.002	22.346*	-0.122	-0.120	22.400	22.397*	-0.003	22.275*	-0.125	-0.122
	D	· CID					0.0=0	0 0==			0.005		0.0=0	0.0=0
_	RM	SE			0.005		0.072	0.075			0.007		0.072	0.072

Table 3. Comparison of the rovibrational energies  $E^v_{\rm nT(Q)}$  and  $E^v_{12}$ , for  $ortho{\rm H}_2{\text{-CO}}$  calculated with the  $V_{\rm nT(Q)}$  and  $V_{12}$ , respectively. The differences of the corresponding energies are denoted by  $\Delta^v_{12,{\rm nT(Q)}} = E^v_{\rm nT(Q)} - E^v_{12}$ . The values of  $E^v_{\rm nT(Q)}$  and  $E^v_{12}$  are given relative to the energies of the ground states, which amount to 98.731 (97.967) cm<sup>-1</sup> and 98.530 (97.789) cm<sup>-1</sup> for v=0 and 1, respectively, for  $E^v_{\rm nT(Q)}$  ( $E^v_{12}$ ). Note that the zero of energy is the same as in Table 2, i.e., for  $H_2(v_1=0,j_1=0)$  and  $CO(v_2=0$  or  $v_2=1,j_2=0$ ) separated to infinity. The resonance states are denoted with asterisks. RMSEs are calculated for the energies corresponding to the bound states in the case of  $V_{12}$ . The results for  $V_{12}$  are taken from Ref. [15]. The experimental energy pattern for  $ortho{\rm H}_2{\text{-CO}}$  is not available in the literature. The unit of energy is cm<sup>-1</sup>.

$\overline{J}$	$\overline{P}$	$n_{J,P}$	$E_{12}^{0}$	$E_{\rm nT(Q)}^0$	$\Delta^0_{12,nT(Q)}$	$E_{12}^{1}$	$E^1_{\rm nT(Q)}$	$\Delta^1_{12,\mathrm{nT}(\mathrm{Q})}$
0	1	1	5.694	$\frac{11(Q)}{5.656}$	-0.038	5.693	5.678	-0.015
0	1	2	18.962	18.831	-0.131	18.870	18.763	-0.107
0	1	3	24.472	23.883	-0.589	24.597	23.910	-0.687
0	2	1	0.387	0.442	0.055	0.356	0.311	-0.045
0	2	2	1.171	1.259	0.088	1.226	1.430	0.204
0	2	3	4.322	4.368	0.046	4.325	4.404	0.079
0	2	4	13.062	13.091	0.029	12.982	13.033	0.051
0	2	5	18.854	18.702	-0.152	18.767	18.651	-0.116
1	1	1	0.819	0.806	-0.013	0.844	0.845	0.001
1	1	2	4.339	4.377	0.038	4.316	4.376	0.060
1	1	3	7.576	7.551	-0.025	7.566	7.561	-0.005
1	1	4	11.556	11.518	-0.038	11.474	11.455	-0.019
1	1	5	13.252	13.224	-0.028	13.179	13.184	0.005
1	1	6	13.563	13.472	-0.091	13.517	13.444	-0.073
1	1	7	19.422	19.072	-0.350	19.425	19.133	-0.292
1	1	8	20.611	20.330*	-0.281	20.617	20.344*	-0.273
1	2	1	0.000	0.000	0.000	0.000	0.000	0.000
1	2	2	1.686	1.836	0.150	1.771	1.693	-0.078
1	2	3	2.036	2.026	-0.010	2.004	2.251	0.247
1	2	4	4.854	4.897	0.043	4.830	4.900	0.070
1	2	5	5.573	5.610	0.037	5.563	5.622	0.059
1	2	6	11.578	11.539	-0.039	11.495	11.474	-0.021
1	2	7	12.364	12.379	0.015	12.283	12.322	0.039
1	2	8	14.105	14.008	-0.097	14.074	14.006	-0.068
1	2	9	15.082	15.067	-0.015	15.004	15.012	0.008
1	2	10	18.421	18.222	-0.199	18.360	18.196	-0.164
1	2	11	20.294	19.668	-0.626	20.419	19.828	-0.591
1	2	12	$23.743^*$	23.361*	-0.382	23.679*	23.394*	-0.285
1	2	13	24.182*	23.539*	-0.643	24.289*	23.672*	-0.617
_								
2	1	1	2.953	2.927	-0.026	2.976	2.961	-0.015
2	1	2	4.216	4.219	0.003	4.220	4.243	0.023
2	1	3	5.509	5.529	0.020	5.494	5.537	0.043
2	1	4	10.579	10.549	-0.030	10.574	10.554	-0.020
2	1	5	11.586	11.606	0.020	11.487	11.538	0.051
2	1	6	14.275	14.226	-0.049	14.194	14.163	-0.031
2	1	7	15.334	15.297	-0.037	15.260	15.253	-0.007
2	1	8	15.797	15.673	-0.124	15.735	15.629	-0.106
2	1	9	19.473	19.266	-0.207	19.397	19.232	-0.165
_2	1	10	24.449*	23.683*	-0.766	24.551*	23.808*	-0.743

Table 3. Continuation.

J	P	$n_{J,P}$	$E_{12}^{0}$	$E_{\rm nT(Q)}^0$	$\Delta^0_{12,\mathrm{nT(Q)}}$	$E_{12}^{1}$	$E^1_{\rm nT(Q)}$	$\Delta^1_{12,\mathrm{nT(Q)}}$
2	2	1	1.251	1.241	-0.010	1.246	1.236	-0.010
$\overline{2}$	$\overline{2}$	$\overline{2}$	2.701	2.795	0.094	2.745	2.816	0.071
2	$\overline{2}$	3	4.157	4.251	0.094	4.224	4.349	0.125
2	$\frac{2}{2}$	4	4.683	4.642	-0.041	4.636	4.638	0.002
$\frac{2}{2}$	2	5	6.665	6.682	0.017	6.636	6.683	0.002 $0.047$
2								
$\frac{2}{2}$	$\frac{2}{2}$	6	7.730	7.743	0.013	7.719	7.751	0.032
2	2	7	12.158	12.185	0.027	12.056	12.106	0.050
2	2	8	12.901	12.913	0.012	12.818	12.850	0.032
2	2	9	14.358	14.292	-0.066	14.280	14.235	-0.045
2	2	10	17.099	16.976	-0.123	17.069	16.974	-0.095
2	2	11	17.918	17.832	-0.086	17.849	17.792	-0.057
2	2	12	19.497	19.343	-0.154	19.420	19.296	-0.124
2	2	13	23.900*	23.369*	-0.531	23.885*	$23.465^*$	-0.420
3	1	1	6.099	6.053	-0.046	6.116	6.078	-0.038
3	1	2	6.908	6.900	-0.008	6.915	6.930	0.015
3	1	3	7.710	7.704	-0.006	7.700	7.720	0.020
3	1	4	11.880	11.879	-0.001	11.817	11.836	0.019
3	1	5	12.965	12.988	0.023	12.890	12.927	0.037
3	1	6	14.563	14.495	-0.068	14.537	14.499	-0.038
3	1	7	17.492	17.413	-0.079	17.424	17.364	-0.060
3	1	8	18.419	18.359	-0.060	18.346	18.315	-0.031
3	1	9						
3	1		19.013 23.238*	18.844	-0.169	18.937	18.789	-0.148
3	1	10	23.238	23.232*	-0.006	21.228*	20.994*	-0.234
3	2	1	3.494	3.465	-0.029	3.488	3.453	-0.035
3	2	2	4.353	4.435	0.029	4.392	4.483	0.091
3	2	3						
	2		6.848	6.959	0.111	6.926	7.053	0.127
3	2	4	7.949	7.888	-0.061	7.893	7.867	-0.026
3	2	5	9.454	9.448	-0.006	9.421	9.444	0.023
3	$\frac{2}{2}$	6	10.808	10.792	-0.016	10.800	10.802	0.002
3	2	7	11.944	11.940	-0.004	11.884	11.900	0.016
3	2	8	14.173	14.193	0.020	14.070	14.113	0.043
3	2	9	14.937	14.928	-0.009	14.853	14.866	0.013
3	2	10	16.966	16.840	-0.126	16.904	16.799	-0.105
3	2	11	21.075*	20.882*	-0.193	21.035*	20.886*	-0.149
3	2	12	24.402*	24.288*	-0.114	24.174*	24.159*	-0.015
4	1	1	10.170	10.101	-0.069	10.169	10.094	-0.075
4	1	2	10.472	10.466	-0.006	10.502	10.530	0.028
4	1	3	10.956	10.899	-0.057	10.943	10.917	-0.026
4	1	4	15.042	15.018	-0.024	14.962	14.961	-0.001
4	1	5	15.456	15.438	-0.018	15.395	15.395	0.000
4	1	6	19.296	19.206	-0.090	19.269	19.205	-0.064
4	1	7	21.609*	21.472*	-0.137	21.558*	21.448*	-0.110
4	1	8	22.421*	22.250*	-0.171	22.356*	22.266*	-0.090
4	1	9	22.965*	22.796*	-0.169	22.860*	22.713*	-0.147
4	1	10	25.034*	24.920*	-0.114	24.871*	24.812*	-0.059
-	_							
4	2	1	6.706	6.641	-0.065	6.693	6.591	-0.102
4	2	2	6.824	6.905	0.081	6.875	7.005	0.130
4	2	3	9.832	9.926	0.094	9.880	9.989	0.109
4	2	4	12.035	11.966	-0.069	11.972	11.939	-0.033
4	$\frac{2}{2}$	5	13.167	13.147	-0.020	13.153	13.155	0.002
4	2	6	14.792	14.740	-0.052	14.791	14.757	-0.034
4	2	7	14.792 $15.500$	15.456	-0.032	14.791 $15.441$	15.419	-0.034
4	$\frac{2}{2}$	8	15.300 $17.261$	15.450 $17.258$	-0.044	15.441 $17.157$	15.419 $17.178$	0.022
4	$\frac{2}{2}$	9						
	2		18.059	18.019	-0.040	17.975	17.958	-0.017
4		10	20.436	20.238*	-0.198	20.397	20.225*	-0.172
_4	2	11	23.295*	23.285*	-0.010	23.136*	23.136*	0.000

Table 3. Continuation.

$\overline{J}$	$\overline{P}$	20 7 70	$E_{12}^{0}$	$E_{\rm nT(Q)}^0$	$\Lambda^0$	$E_{12}^{1}$	$E^1_{\rm nT(Q)}$	Λ1
		$n_{J,P}$			$\Delta_{12,nT(Q)}^{0}$			$\Delta^{1}_{12,nT(Q)}$
5	1	1	14.788	14.767	0.021	14.809	14.741	-0.000
5	1	2	14.969	14.911	-0.058	14.981	14.999	0.018
5	1	3	15.362	15.215	-0.147	15.345	15.231	-0.114
5	1	4	18.563	18.518	-0.045	18.481	18.458	-0.023
5	1	5	19.366	19.280	-0.086	19.318	19.252	-0.066
5	1	6	24.344*	24.252*	-0.092	24.282*	24.214*	-0.068
_	_							
5	2	1	10.121	10.165	0.044	10.170	10.182	0.012
5	2	2	10.878	10.801	-0.077	10.882	10.854	-0.028
5	2	3	13.113	13.169	0.056	13.121	13.195	0.074
5	2	4	16.518	16.473	-0.045	16.453	16.441	-0.012
5	2	5	18.000	17.935	-0.065	18.009	17.963	-0.046
5	2	6	19.628	19.528	-0.100	19.638	19.555	-0.083
5	2	7	20.091	$19.997^*$	-0.094	20.022	19.954	-0.068
5	2	8	21.310*	21.270*	-0.040	21.208*	21.192*	-0.016
5	2	9	22.225*	$22.135^*$	-0.090	22.141*	22.081*	-0.060
6	1	1	19.773	19.740	-0.033	19.834	19.802	-0.032
6	1	2	20.323	20.195*	-0.128	20.306	20.205*	-0.101
6	1	3	20.835*	20.649*	-0.186	20.802*	20.654*	-0.148
6	1	4	22.896*	22.798*	-0.098	22.825*	22.750*	-0.075
6	1	5	24.224*	23.992*	-0.232	24.198*	24.020*	-0.178
6	2	1	14.250	14.286	0.036	14.323	14.347	0.024
6	2	2	15.909	15.774	-0.135	15.915	15.813	-0.102
6	2	3	16.927	16.929	0.002	16.896	16.920	0.024
6	2	4	21.165*	21.142*	-0.023	21.109*	21.113*	0.004
6	2	5	23.889*	23.758*	-0.131	23.900*	23.790*	-0.110
6	2	6	25.364*	25.262*	-0.102	25.270*	25.151*	-0.119
6	2	7	26.358*	26.256*	-0.102	26.295*	26.194*	-0.101
7	1	1	25.338*	25.302*	-0.036	25.419*	25.319*	-0.100
7	1	2	26.302*	26.094*	-0.208	26.300*	26.113*	-0.187
7	2	1	19.099	19.125	0.026	19.205	19.226	0.021
7	2	2	21.464*	21.335*	-0.129	21.392*	21.300*	-0.092
7	2	3	21.690*	21.534*	-0.156	21.710*	21.570*	-0.140
7	2	4	26.068*	26.040*	-0.028	26.003*	25.999*	-0.004
•	_	-		0.0 -0	5.520			0.004
8	2	1	24.497*	24.489*	-0.008	24.632*	24.631*	-0.001
8	$\overline{2}$	2	26.822*	26.642*	-0.180	26.732*	26.571*	-0.161
8	$\frac{1}{2}$	3	31.335*	31.260*	-0.075	31.259*	31.206*	-0.053
Ŭ	_	,	3300	200	2.0.3	5 = . <b>=</b> 00	3-1-00	2.000
	RM	SE			0.122			0.122
_					<b>-</b>			<b>-</b>

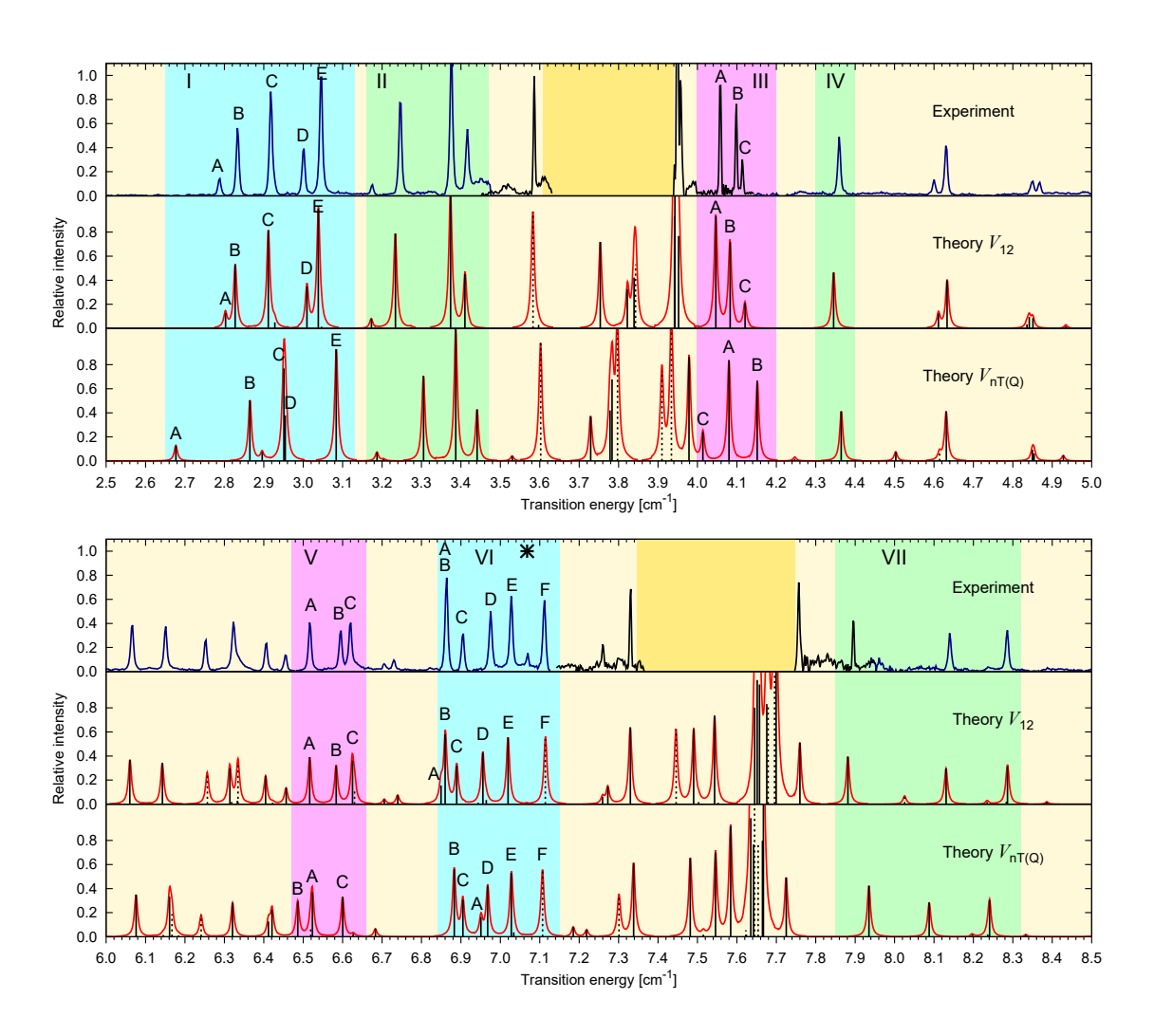


Figure 2. Comparison of the selected ranges of the infrared spectra of  $paraH_2$ –CO calculated from the  $V_{\rm nT(Q)}$  surfaces for T=49 K (bottom part of each panel) with the experimental data from Refs. [15, 59] (upper part) and the theoretical one calculated from the  $V_{12}$  surfaces in Refs. [15, 30] (central part). The experimental spectrum is shifted by the value of the  $v_2=1\leftarrow 0$  transition in the isolated CO equal to 2143.272 cm<sup>-1</sup>. The experimental spectrum recorded at the gas pressure of 3.5 Torr and T=49 K (blue line) was merged with the spectrum recorded at 1.1 Torr and 47.5 K (black line). The dashed lines on the theoretical parts of the plot denote transitions that involve at least one resonance state. The calculated transitions with relative intensities larger than 0.01 are plotted. The yellow rectangles indicate gaps in the experimental data due to the strong CO monomer lines, whereas the transition indicated by asterisks are the R-branch transitions of the isotopologues in natural abundance. Shaded cells indicate parts of the spectra discussed in the text. They are green in the case if all three spectra resemble each other to a degree which allows unambiguously assign the experimental one. If the transitions calculated from  $V_{\rm nT(Q)}$  are significantly shifted with respect to those calculated from from  $V_{12}$ , the cells are shaded in blue. In the case when the order of the  $V_{\rm nT(Q)}$  peaks is changed in comparison with the  $V_{12}$  ones, the cells are magenta shaded.

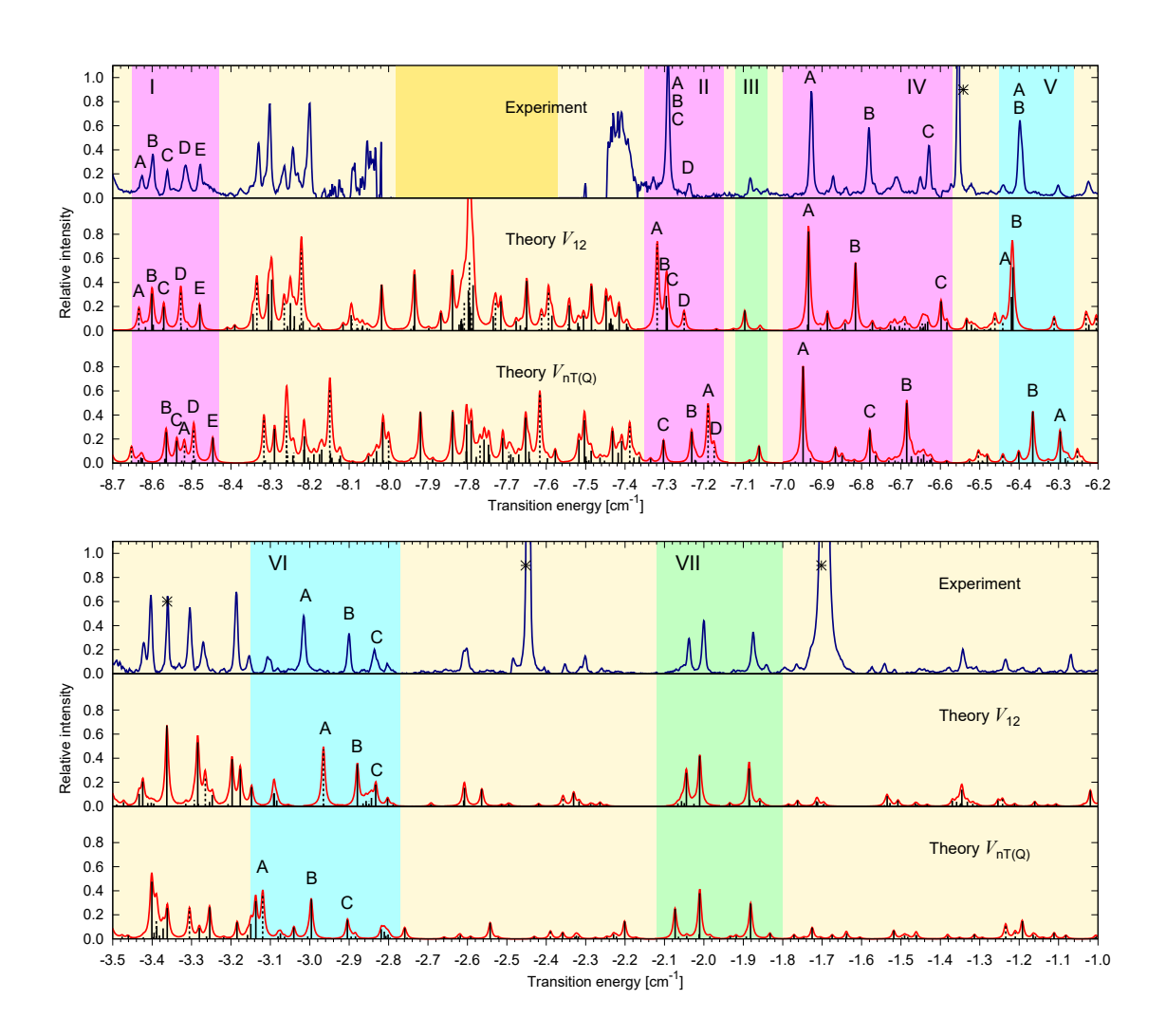


Figure 3. Comparison of the selected ranges of the infrared spectra of  $ortho H_2$ –CO calculated from the  $V_{\rm nT(Q)}$  surfaces for T=49 K (bottom part of each panel) with the experimental data from Ref. [15] (upper part) and the theoretical one calculated from the  $V_{12}$  surfaces from Ref. [15, 30] (central part). The experimental spectrum is shifted by the value of the  $v_2=1\leftarrow 0$  transition in the isolated CO equal to 2143.272 cm<sup>-1</sup>. The detailed information about the symbols and the colours of shading is given in the caption of Fig. 2.